Classification
Physics Abstracts
61.16D — 73.40L — 81.15H

Epitaxial orientation of β-$FeSi_2$/Si heterojunctions obtained by RTP chemical vapor deposition

I. Berbezier(*), J.L. Regolini and C. d'Anterroches

CNET, France Télécom, Chemin du Vieux Chêne, BP. 98, 38243 Meylan Cedex, France

(Received 8 December 1992, accepted 22 February 1993)

Abstract . — In recent years the semiconducting phase of iron silicide β-$FeSi_2$ has attracted interest. Promising applications of a great deal of β-$FeSi_2$/Si heterojunctions are reported in semiconductor technology due to the 0.89 eV direct band gap of β-$FeSi_2$. Most of the papers devoted to this material present three different deposition modes, i.e. MBE, Solid Phase Epitaxy (SPE) and Reactive Deposition Epitaxy (RDE). The epitaxy of very thin layers of β-$FeSi_2$ has already been reported on (111) and (001) silicon substrates. This paper presents an original application of Chemical Vapor Deposition (CVD) for the growth of β-$FeSi_2$ using Rapid Thermal Processing (RTP). The results presented here mainly concern the epitaxial orientations and the morphology of β-$FeSi_2$ on silicon. The different epitaxial relationships are experimentally distinguished by the use of transmission electron diffraction (TED) and microscopy (TEM). Thick β-$FeSi_2$ layers (> 100 nm) have been selectively grown by RTP chemical vapor deposition on patterned (111) and (001) silicon wafers and under different experimental conditions. They are polycrystalline with large grains (about 1 μm) and mainly epitaxial. The main epitaxial relationship found is (220) β-$FeSi_2$ // (111) Si named type B in the literature. An important result is the flatness of the interface under each β-$FeSi_2$ grain which presents large areas (about 50 nm) without any monoatomic step. This result seems to be an advantage of the promising chemical vapor deposition process used which minimizes the interdiffusion processes at the interface.

1. Introduction.

Iron disilicide is known to crystallize under two phase forms (i) the tetragonal α-$FeSi_2$, stable at high temperature and (ii) the orthorhombic β-$FeSi_2$, stable below 950 °C with the following lattice parameters: a = 9.863 Å, b = 7.791 Å and c = 7.833 Å and belonging to the space group Cmca (n° 64). The atomic structure of this orthorhombic phase has been described by Dusausoy *et al.* [1]. Data show that the natural crystal is very imperfect: numerous crystal twinnings and microplanar defects identified as intrinsic stacking faults have been reported [2,3].

(*) Permanent address: CRMC2, CNRS, Faculté des Sciences de Luminy, 13288 Marseille Cedex 9, France

Several papers concern thin β-$FeSi_2$ layers epitaxially grown by solid phase reaction onto (111) and (001) silicon substrates [4-6]. The limit thickness of epitaxial layers seems to be about 10 nm. The three deposition modes currently used are reactive deposition epitaxy (RDE), molecular beam epitaxy (MBE) and solid phase epitaxy (SPE). However, no study relates the growth of thick epitaxial layers (> some tens of nanometers) without crystalline defects. Moreover, even for very thin layers, β-$FeSi_2$/Si interfaces are rough (numerous monoatomic steps are observed over a small field). The presence of crystallographic defects and the roughness of the interface remain the major problems concerning possible micro-electronic applications of β-$FeSi_2$/Si heterojunctions.

In this paper, a new approach to the formation of thick iron silicide layers with chemical vapor deposition using an iron chlorinated compound is used and shows itself to be an interesting candidate for β-$FeSi_2$ deposition. Indeed, shorter deposition times and easier manipulation (without the technology of ultra high vacuum) allow thick layers to be obtained with interesting microstructural and semiconducting porperties. Although polycrystalline (with different azimuthal orientations), the layers possess very flat interfaces under each epitaxial grain.

The purpose of this paper is to compare the experimental epitaxial relationships found between β-$FeSi_2$ grains and (111) or (001) silicon substrates with the theoretical ones. Different anomalies are described. All the results presented are obtained by TEM and TED.

2. Experimental.

In this work chemical vapor deposition (CVD) was used to grow stoichiometric β-$FeSi_2$ using Rapid Thermal Processing which has been termed Limited Reaction Processing (LRP) [7]. Briefly, the reactor is an air cooled quartz tube where a 4″ Si wafer is self-supported and heated by a set of powerful lamps. One of the problems of silicide CVD is to find a metal precursor which is easy to handle and safe. The idea was to use *in situ* metal chlorination to obtain these precursors [8]. Thus, an iron source was set up, external to the reactor, which consists of a reaction chamber containing high purity iron wire and where Cl_2 gas diluted in Ar passes through while wire is heated to above 300 °C. It has been shown in a previous paper [9] that $FeCl_3$ is produced and transported in the reaction chamber.

The reactor feeding gases are SiH_4, H_2, He and (in a separate line) $FeCl_3$ diluted in Ar. All samples are subjected to a chemical cleaning followed by an *in situ* thermal cleaning consisting of 30 sec at 1000 °C under 1 Torr of H_2. The deposition cycles are fast for this type of material, around 1 to 10 min at temperatures within 750 and 850 °C. No post deposition annealing followed for any of the samples. Detailed experimental conditions have already been presented in [9].

The studied β-$FeSi_2$ layers were deposited at 750 °C or 850 °C for 1 or 2 min, by deposition of Fe or codeposition of Fe/Si with calculated stoechiometric composition. Their thicknesses vary between 50 and 150 nm.

TEM samples were prepared either by (i) mechanical thinning followed by ion milling for cross sectional analyses or by (ii) mechanical thinning followed by chemical thinning for plane view analyses. Wafers are cut up with a diamond saw along <112> and <110> crystallographic directions.

3. Crystallographic description of β-$FeSi_2$/Si (111).

When deposited on (111) silicon, two β-$FeSi_2$ crystallographic planes (202) and (220) are currently reported to match the substrate [10,11]. The lattice mismatches are then respectively 1.45% and 2% along the [112] silicon axis (Fig. 1). In this case the epitaxial relationships (Fig. 2) are the following:

- Type A: [111] Si at 13.1° of [10-1] β-$FeSi_2$
  (the exact parallel axis is [1,0,-1.26])
  [1-10] Si // [010] β-$FeSi_2$
  [11-2] Si // [-101] β-$FeSi_2$ with (111) Si // (202) β-$FeSi_2$

- Type B: [111] Si at 13.4° of [-110] β-$FeSi_2$
  (the exact parallel axis is [1,-1.26,0])
  [1-10] Si // [001] β-$FeSi_2$
  [11-2] Si // [1-10] β-$FeSi_2$ with (111) Si // (220) β-$FeSi_2$

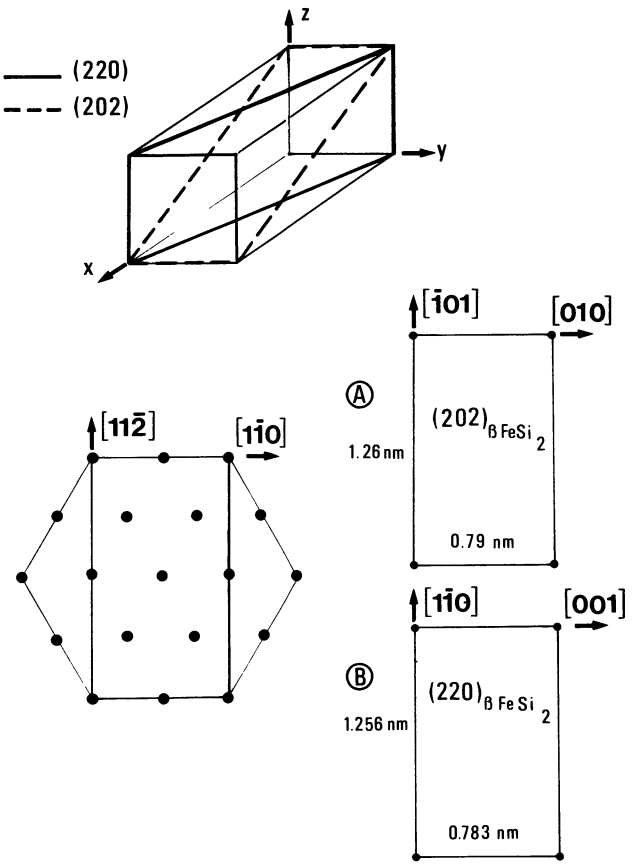

Fig. 1. — β-$FeSi_2$ lattice cell. (A) (202) and (B) (220) β-$FeSi_2$ matching faces on (111) silicon substrate.

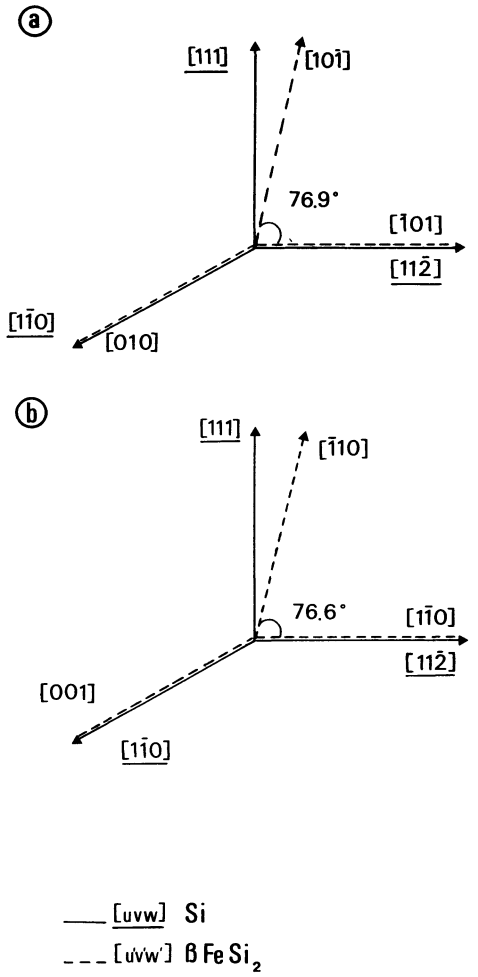

Fig. 2. — Crystallographic directions of β-$FeSi_2$/Si for (a) type A and (b) type B epitaxy.

The main crystallographic directions on the (111) Si face and on the (202) or (220) β-$FeSi_2$ matching faces are represented schematically in figure 3. In order to have a complete crystallographic description of the system, the samples are experimentally analysed along the [111], [1-10] and [11-2] Si axes.

Concerning the plane view observations (along the [111] Si) it must be recalled that Moiré fringes spacings are very sensitive to the types of epitaxy and are a very simple way to differenciate two types of epitaxy. Indeed spacings that correspond to double diffraction of (i) (220) Si and (040) β-$FeSi_2$ (type A epitaxy) and of (ii) (220) Si and (004) β-$FeSi_2$ (type B epitaxy) should be respectively 13.4 nm and 9.9 nm. The two theoretical diffraction patterns expected along this zone axis are represented schematically in figure 4. Considering the threefold symmetry of the (111) Si plane and the twofold symmetry of (220) and (202) β-$FeSi_2$ planes there are three equivalent orientations twinned by 60°. They are represented by three different sets of points on the diagrams. Furthermore, it can be seen that the only difference (observable by TED) between the two theoretical diagrams is the presence of {114} β-$FeSi_2$

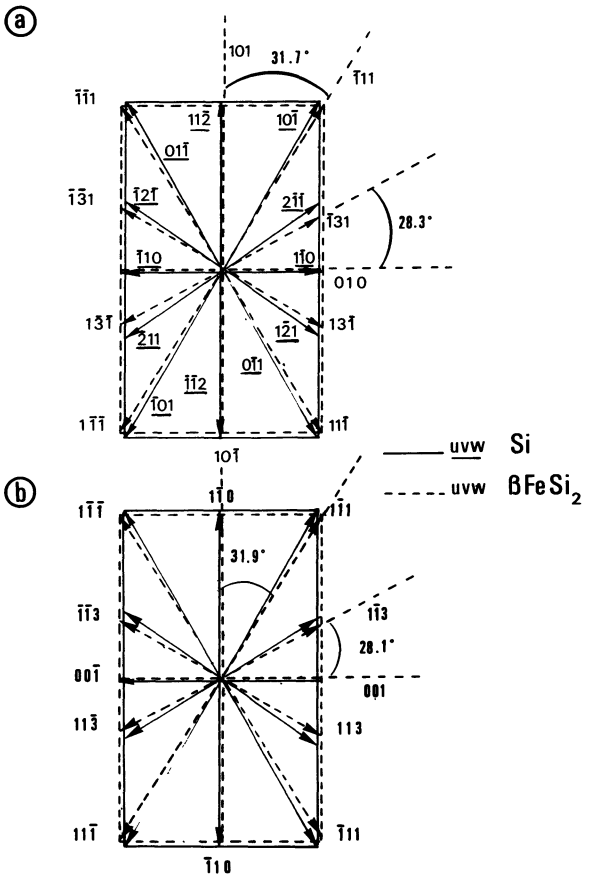

Fig. 3. — Representation of the crystallographic directions of (111) Si face // to (a) (202) and (b) (220) β-$FeSi_2$ face.

planes, representative of the [110] β-$FeSi_2$ azimuthal direction. However, the tilt angle between the [111] Si axis and the [10-1] or [1-10] β-$FeSi_2$ axis (about 13°) should induce a significant decrease in spot intensities.

Theoretical TED diagram with the electron beam along [11-2] Si and [110] β-$FeSi_2$ is presented in figure 5a. The diagram expected along [101] β-$FeSi_2$ can be deduced from figure 5a by exchanging k and l indices and with {141} planes extincted.

Theoretical TED diagram with the electron beam along [1-10] Si and [001] β-$FeSi_2$ is presented in figure 5b. Along this direction it is impossible to distinguish the type of epitaxy and a very similar diagram is obtained along the [010] β-$FeSi_2$ by exchanging k and l indices of the planes. However it is possible to remove the 180° ambiguity, coming from the possibility of the β-$FeSi_2$ matching face to rotate of 180° about the [111] silicon axis.

Considering now the effect of a rotation of 60° it can be seen that another azimuthal orientation must be obtained which is [1-10] Si // <111> β-$FeSi_2$ (Fig. 6a) and [11-2] Si // <113> (or <131>) β-$FeSi_2$. These new relationships are easily distinguished from those described above and illustrate the presence of the three variants.

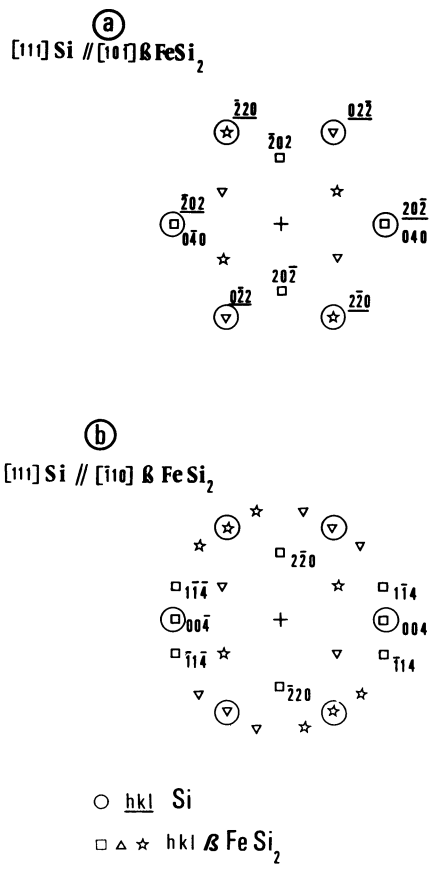

Fig. 4. — Theoretical TED diagram with the electron beam along the [111] Si and along (a) [10-1] β-$FeSi_2$; (b) [-110] β-$FeSi_2$.

4. Results: β-$FeSi_2$/Si (111).

Two main results are obtained from the study of the deposition experimental conditions: (i) an annealing treatment of the layers after deposition does not influence the crystalline quality of β-$FeSi_2$, (ii) codeposition with approximat stoechiometric composition increases greatly the flatness of the interface. The layers presented here were obtained by codeposition at 750 °C for 2 min.

Experimentally, complex diffraction diagrams are often obtained from β-$FeSi_2$ layers (100 nm thick), since various grains with different azimuthal orientations are currently intercepted in selected areas (several micrometers). Plane view TEM observations show that the grain sizes are about 0.1 - 0.3 μm (Fig. 7) and that the major part of the grains is epitaxially grown (revealed on the image by the presence of Moirés fringes). Thinner layers (about 50 nm thick) present much larger epitaxial areas, about several micrometers.

All the observations show that the most visible spacing experimentally measured is 9.3 nm and corresponds to type B epitaxy. In contrast, a corresponding TED diagram (Fig. 8) reveals the extinction of the <114> β-$FeSi_2$ planes and should correspond to [101] β-$FeSi_2$ zone axis.

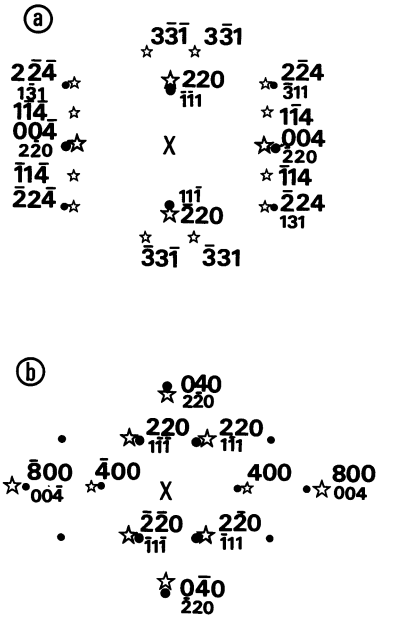

Fig. 5. — Theoretical TED diagram with the electron beam along (a) [11-2] Si // [1-10] β-$FeSi_2$ and (b) [110] Si // [001] β-$FeSi_2$. Points and indices of small size represent Si planes; stars and indices of larger size represent β-$FeSi_2$ planes. This representation is adopted for all the diagrams presented up to the end of the paper.

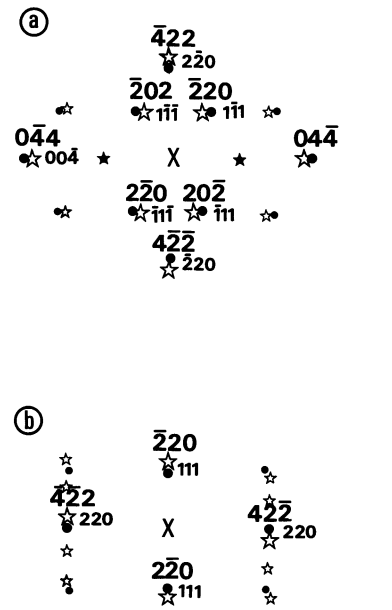

Fig. 6. — Theoretical TED diagram with the electron beam along (a) [110] Si // [-111] β-$FeSi_2$ and (b) [11-2] Si // [113] β-$FeSi_2$.

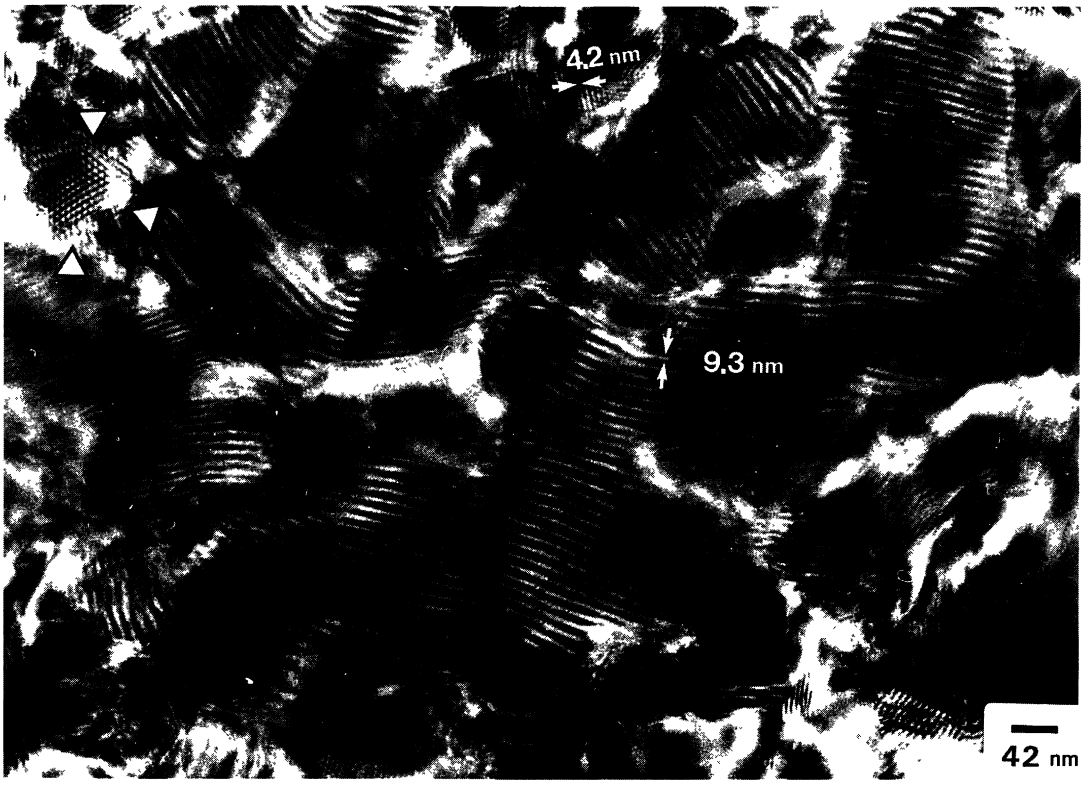

Fig. 7. — Typical TEM plane view. The main fringes spacing is 9.3 nm. Some grains exhibit Moirés fringes rotated by 60° from each other (indicated by arrows) with a 4.2 nm spacing.

However, we have proposed that the tilt angle between the microscope axis and the [110] β-$FeSi_2$ zone axis could explain the extinction of the <114> β-$FeSi_2$ planes. Thus, the epitaxy observed is most probably of type B. The presence of the three variants is demonstrated by the TED diagram.

Three series of Moiré fringes twinned by 60° and spaced approximately at 4 nm are frequently observed (Fig. 7). This observation shows that 60° lattice rotations occur in our samples. Three hypotheses can explain the fringes observed:

(i) the double diffraction of (112) Si with (220) (or (202)) β-$FeSi_2$ which leads to spacing of 4 and 3.8 nm respectively. These two epitaxial orientations cannot be distinguished due to measurement imprecision.

(ii) the double diffraction of (220) Si with (422) β-$FeSi_2$ which leads to Moiré fringes spaced at 4.4 nm.

(iii) a small disorientation of 2° between (220) Si and (004) β-$FeSi_2$ induces Moiré fringes of 4.9 nm. Such a disorientation has already been observed on other samples.

In conclusion, plane view experiments mainly reveal the presence of the three variants of type B epitaxy.

Cross-sectional information is obtained along [11-2] Si and [1-10] Si. Conventional TEM observations confirm the 100 nm mean thickness of the β-$FeSi_2$ layers and indicate their continuity (Fig. 9). Unfortunately, the 3-D growth tendency results in a rough surface and irregular

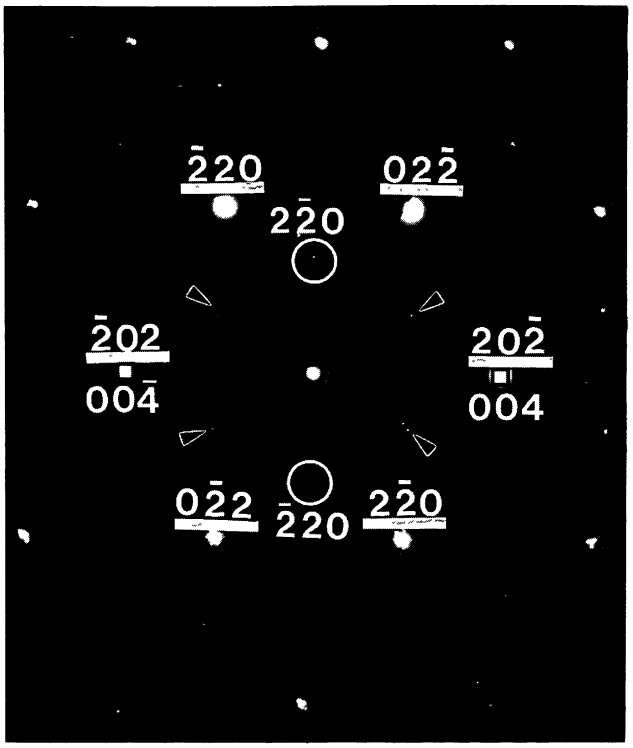

Fig. 8. — Experimental TED pattern obtained with the electron beam along [111] Si. Only one domain is indexed, the two others are indicated by arrows.

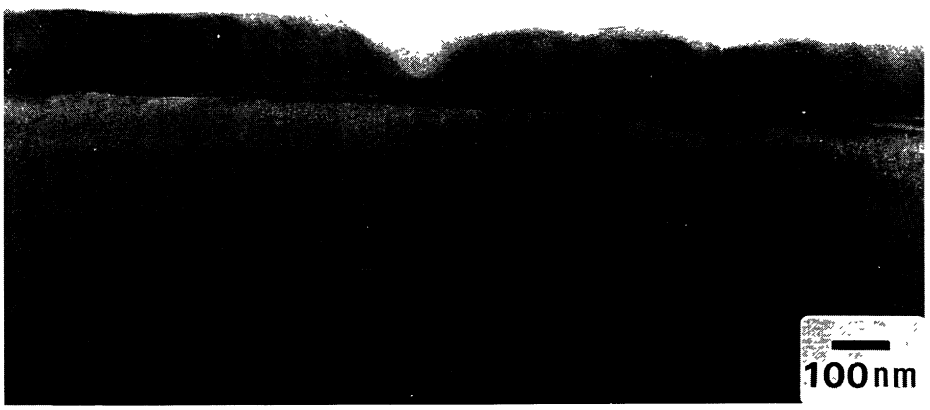

Fig. 9. — Overall cross-sectional image of the layer.

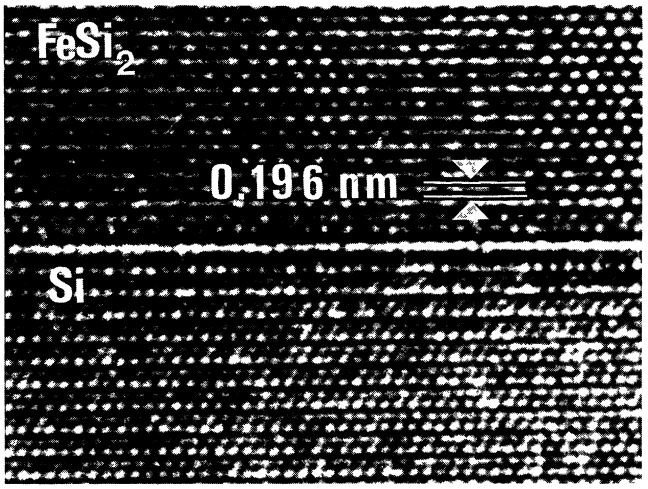

Fig. 10. — High resolution cross-sectional image of Si/β-$FeSi_2$ interface. The electron beam is along [11-2] Si axis.

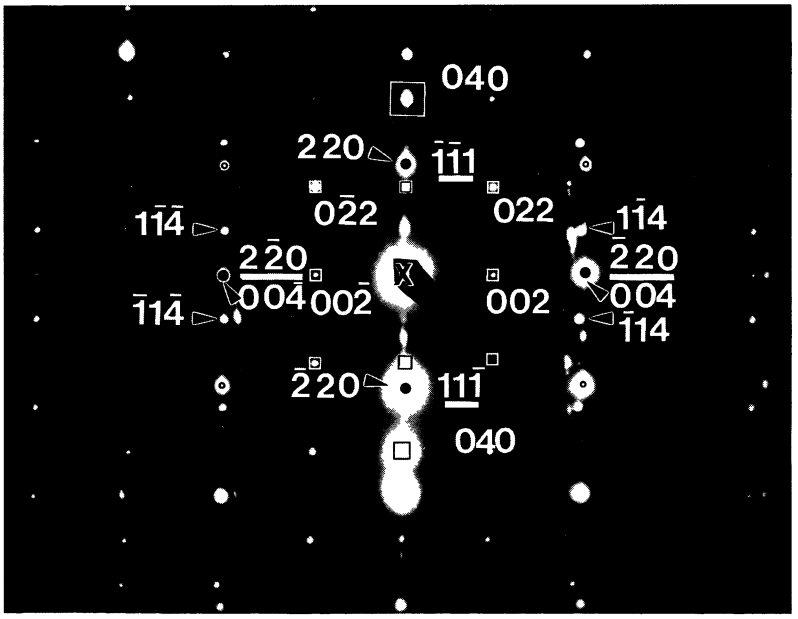

Fig. 11. — Typical TED pattern with the electron beam along [11-2] Si and intercepting two $FeSi_2$ grains with azimuthal orientations. Indexed silicon planes are underlined. Narrows and squares indicate respectively the planes in the [110] and [100] β-$FeSi_2$ azimuthal orientations.

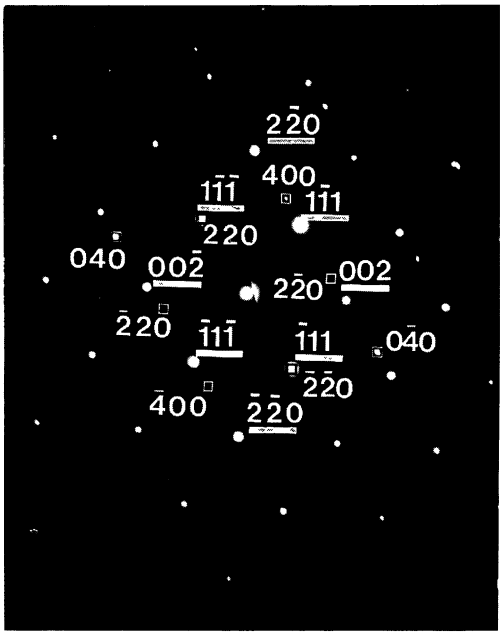

Fig. 12. — Typical TED pattern obtained with the electron beam along [110] Si // [001] β-$FeSi_2$. Indexed silicon planes are underlined and quares indicate the $FeSi_2$ planes.

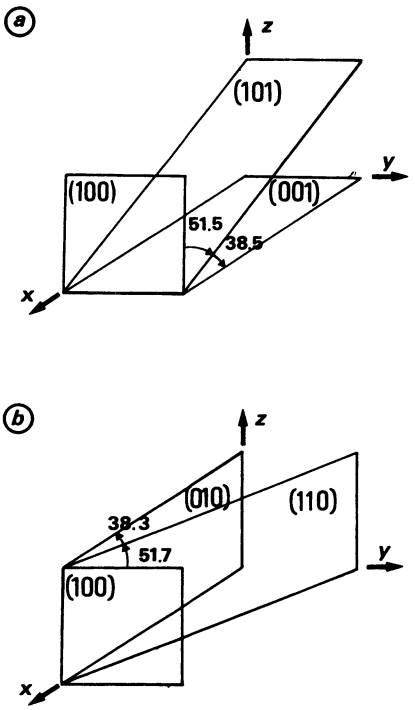

Fig. 13. — Schematization of the rotations observed in our samples about (a) [010] and (b) [001] β-$FeSi_2$.

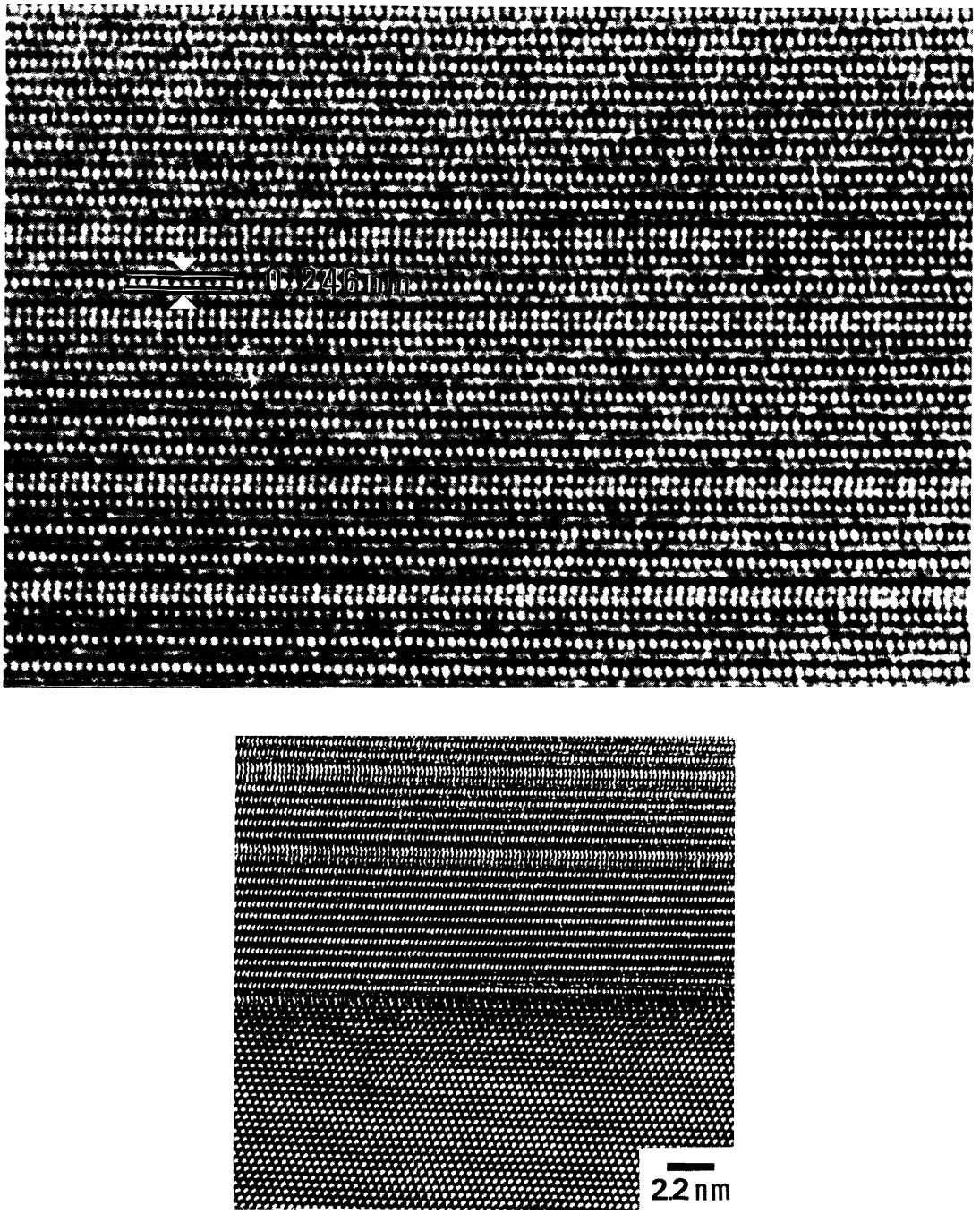

Fig. 14. — High resolution image showing periodic stacking faults in the (100) β-$FeSi_2$ planes.

thickness. However, a very important result to emphasize is the flatness of the interface under each β-$FeSi_2$ grain. Quite large areas of 50 nm are currently observed without any monoatomic

step. A high resolution image of the interface (Fig. 10) shows the abruptness of the contact area.

A typical experimental pattern obtained along the [11-2] Si axis is presented in figure 11. It reveals the presence of two different epitaxial relationships: (i) type B epitaxy (identification of (114) β-$FeSi_2$ planes) and (ii) type D epitaxy (described later).

Considering now TED along the [1-10] Si axis, it must be noted that the theoretical diagram presented in figure 5b has never been observed in our samples and to our knowledge, it has never been observed in the literature. Indeed, the most commonly observed epitaxial relation is presented in figure 12. It reveals a rotation of 180° about [111]Si of the β-$FeSi_2$ matching cell. The presence of the three variants already mentioned is confirmed on some TED diagrams which exhibit two grains with [001] and [111] azimuthal orientations, respectively.

Two different azimuthal orientations named type C and type D and corresponding to rotations of respectively 51.5° and 38.5° about the [001] (or [010]) β-$FeSi_2$ axis are observed (Fig. 13). They are described by the following relationships:

- Type C: [111] Si // [100] β-$FeSi_2$ with (111) Si // (400) β-$FeSi_2$
  [1-10] Si // [001] (or [010]) β-$FeSi_2$
  [1-12] Si // [010] (or [001]) β-$FeSi_2$

The lattice mismatches are: 1.45% or 2% along [1-10] Si and 17.14% or 17.74% along [1-12] Si.

- Type D: [111] Si // [001] (or [010]) β-$FeSi_2$
  with (111) Si // (004) (or (040)) β-$FeSi_2$
  [1-10] Si // [001] (or [010]) β-$FeSi_2$
  [1-12] Si // [100] β-$FeSi_2$

The lattice mismatches are: 1.45% or 2% along [110] Si and -25.84% along [112] Si.

A high resolution image of type C epitaxy (Fig. 14) reveals (i) the flatness of the interface and (ii) the presence of stacking faults in the (100) planes. It must be noted that similar defects have been identified by Zheng *et al.* (2) as (100) [011]/2 intrinsic stacking faults with an average spacing between defects of 20 Å. In our case the defects arise every other plane and create a 2×1 supercell in the [0vw] direction. Others samples prepared by SPE present a 2×2 supercell in large grains. High resolution TEM images are presently being analysed by image processing and simulated by the multislice method.

5. Crystallographic description of β-$FeSi_2$/Si (001).

Concerning the deposition on a (001) silicon substrate the situation seems to be simpler since only the (100) β-$FeSi_2$ plane presents an acceptable mismatch. Two possible azimuthal orientations have already been described by J.E. Mahan [5]. They are designated (Fig. 15):

- type A: [010] or [001] β-$FeSi_2$ // [110] Si and [011] β-$FeSi_2$ // [010] Si. The respective lattice mismatches are 1.45 and 2%

- type B: [010] or [001] β-$FeSi_2$ // [010] Si. The respective lattice mismatches are -4.36 and -3.81%.

The theoretical TED diagram expected along [001] Si for type A and type B are presented in figure 16. Type B, exceptionally present in our samples, will not be detailed here. Concerning type A we present the theoretical cross-sectional TED along [010] Si // [011] β-$FeSi_2$ (Fig. 17) and at 45° along [110] Si // [010] or [001] β-$FeSi_2$ (Fig. 5b).

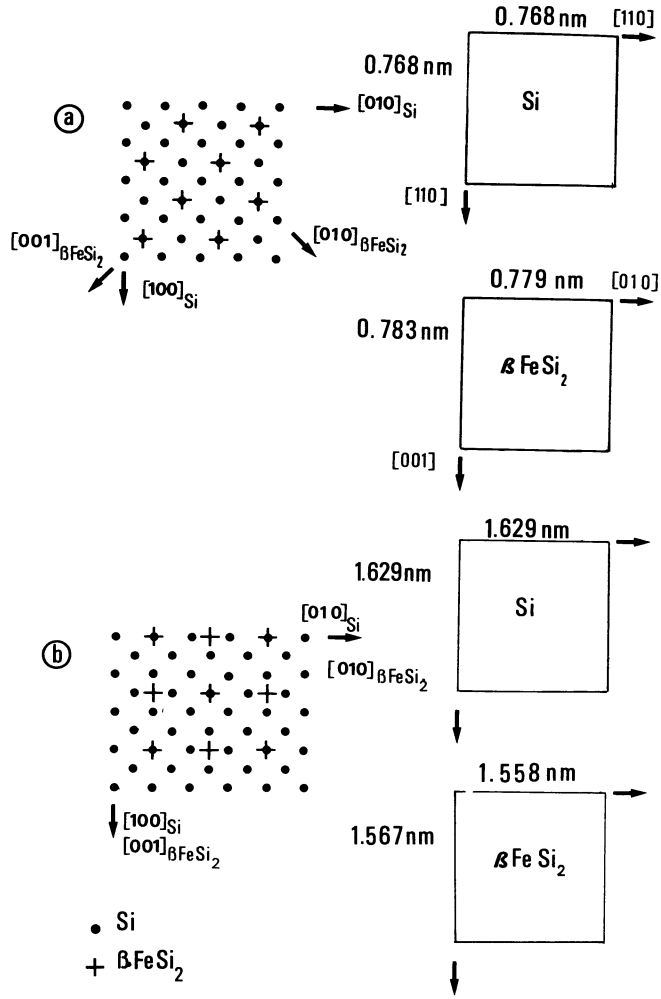

Fig. 15. — Schematization of the lattice matching for (a) type A and (b) type B epitaxy on (001) silicon. They have been already described by J. Mahan (5).

6. Results: β-$FeSi_2$/Si (001).

The β-$FeSi_2$ layers studied here, were obtained by codeposition at 850 °C, for 2 min.

All the samples have been analysed with the electron beam along [001], [010] and [110] Si axis. The layers are continuous (100 nm thick) but polycrystalline with a grain size of about 1 μm. Approximately 50% of the grains are epitaxial in the same way as type A described by J.E. Mahan and they are related to the substrate by the following relationship: (001) Si // (100) β-$FeSi_2$ with [110] Si // [010] or [001] β-$FeSi_2$ (Fig. 18). Type B epitaxy occurs only in one grain and does not seem to be generalized.

Thus, the epitaxial growth on (001) Si seems to be very promising. Indeed, epitaxial layers of 50 nm thick have been grown by SPE with few defects and only type A epitaxy (Fig. 19). Few layers have been obtained by RTP-CVD and a more complete study is required to determine

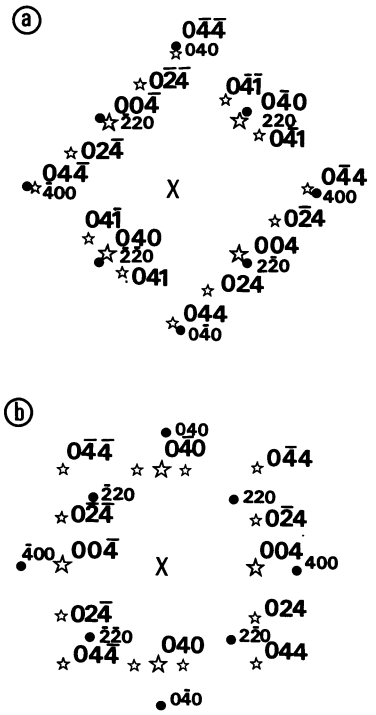

Fig. 16. — Theoretical TED pattern with the electron beam along [100] Si // [100] β-$FeSi_2$ for (a) type A and (b) type B epitaxy on (001) silicon substrate.

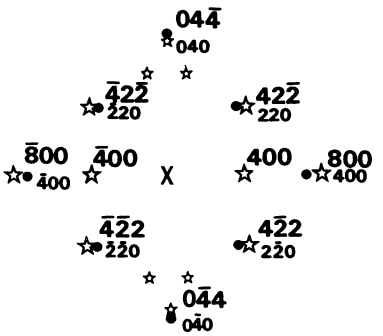

Fig. 17. — Theoretical TED pattern with the electron beam along [010] // [011] β-$FeSi_2$.

the overall crystalline feature of the layers deposited on (001) silicon substrate.

7. Conclusion.

We have shown that the codeposition of β-$FeSi_2$ layers on (111) or (001) silicon substrates

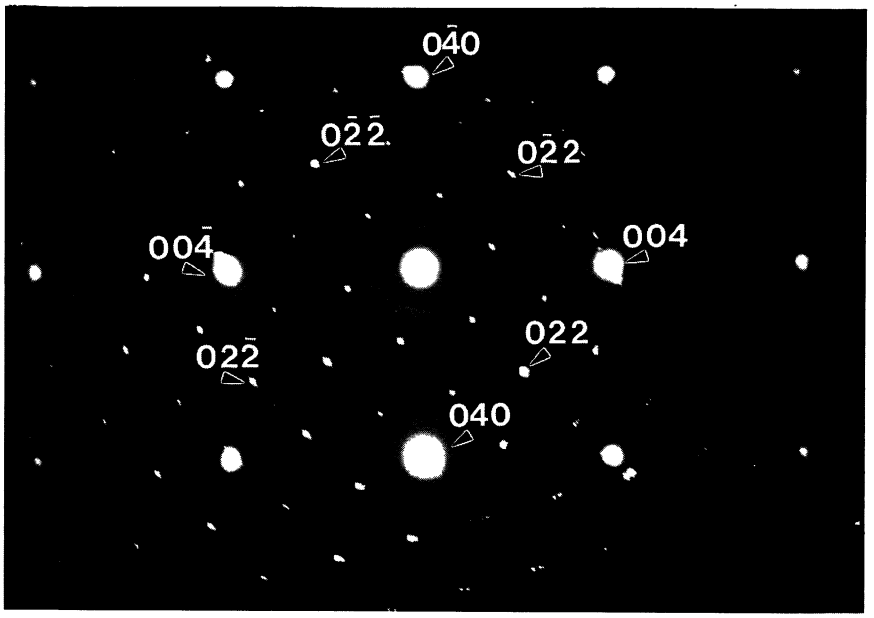

Fig. 18. — Typical experimental TED pattern with the electron beam along [001] Si.

using RTP-CVD induces very low interdiffusion processes at the interface.

Considering deposition on (111) Si we have observed primarily the type B epitaxy with the following relationship: (111) Si // (220) β-$FeSi_2$. The three domains are always present and two problems must be emphasized: (i) the facility of the β-$FeSi_2$ lattice to rotate about [111] and [1-10] Si axis, leading to different azimuthal orientations and (ii) the presence of numerous stacking faults (100) [0vw] creating a 2×1 supercell.

The epitaxial deposition on (001) Si seems to be more promising, considering the single epitaxial relationship found in this study: (001) Si // (100) β-$FeSi_2$ with [110] Si // [010] or [001] β-$FeSi_2$.

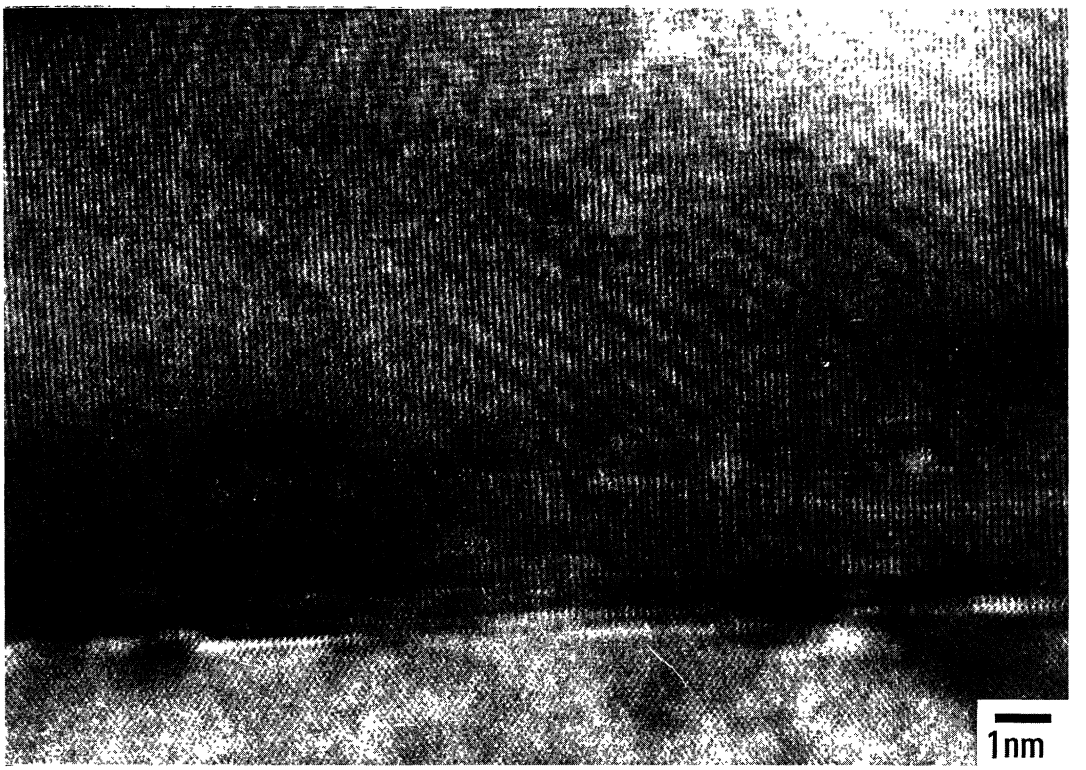

Fig. 19. — Cross-sectional image of the epitaxial β-$FeSi_2$ layer when deposited on (001) silicon substrate. The electron beam is along [110] Si axis.

References

[1] DUSAUSOY Y., PROTAS J., WANDJI R. and ROQUES B., *Acta Cryst.* **B27** (1971) 1209.
[2] ZHENG Y., TACCOEN A. and PETROFF J.F., to be published in *J. Appl. Cryst.*
[3] DUSAUSOY Y. and WANDJI R., *Bull. Soc. Franc. Miner. Crist.* **56** (1970) 93.
[4] CHERIEF N., d'ANTERROCHES C., CINTI R.C., NGUYEN T.A. and DERRIEN J., *Appl. Phys. Lett.* **55** (16) (1989) 1671.
[5] MAHAN J.E., GEIB K.M., ROBINSON G.Y. and LONG R.G., *J. Vac. Sci. Technol.* **OA8** (5) (1990) 3692.
[6] CHEVRIER J., LE THANH V., NITSCHE S. and DERRIEN J., *Appl. Surf. Sci.* **438** (1992) 56.
[7] GIBBONS J.F., GRONET C.M. and WILLIAMS K.E., *Appl. Phys. Lett.* **47** (1985) 721.
[8] BLANQUET E., VAHLAS C., BERNARD C., MADAR R., PALLEAU J. and TORRES J., *J. Physique* C5 **557** (1989).
[9] REGOLINI J.L., TRINCAT F., BERBEZIER I., PALLEAU J., MERCIER J. and BENSAHEL D., CVD-8 (Glasgow Scotland, September 1991) published in *J. Phys. III France.*
[10] DERRIEN J., CHEVRIER J., LE THANH V. and MAHAN J.E., *Appl. Surf. Sci.* **382** (1992) 56.
[11] von KANEL H., HENZ J., OSPELT M. and WACHTER P., *Physica Scripta* **19** (1987) 158.